Fast Simulations of Star Cluster Evolution

Lina Warntoft

Lund Observatory
Lund University

2019-EXA142

Degree project of 15 higher education credits
February 2019

Supervisor: Florent Renaud

Lund Observatory
Box 43
SE-221 00 Lund
Sweden

Abstract

The evolution of globular star clusters tells the history of the formation of galaxies, how stellar streams might have formed and how the future of the Universe might look like. Although the general theoretical background of the evolution is well understood, it is difficult to conduct accurate and realistic computer simulations of objects containing thousands of interacting bodies. This project introduces a new method tackling this issue, treating star clusters as point objects while they are losing stars as a result of tidal stripping. This is all conducted based on the concept of potential escapers. Combining the computational effectiveness of a simplified approximation of a star cluster with the accuracy of an N-body simulation, this project introduces a new option for globular star cluster simulation.

The code written for this model allows to introduce any star cluster into any external potential. The star cluster is then described using five main coupled differential equations: number of stars, half mass radius, total energy, core radius and density profile, which, when integrated using a 4th order Runge-Kutta scheme, allows to model the full evolution of the cluster in less than a minute on a single computer. Tracer particles for potential escapers are implemented so that the tidal stripping works in constant as well as varying tidal fields. The results of this project show that the star loss over time is comparable to the ones conducted using much slower direct N-body simulations, e.g. the step-like loss of stars in elliptical tidal fields, while at the same time having a run-time of about a few minutes. Further development of this method might contribute to the understanding of stellar streams and build-up of stellar populations in galaxies.

Populärvetenskaplig beskrivning

Högt över och långt under den galaktiska disken av Vintergatan svävar gigantiska stjärnhopar som tros ha existerat sedan begynnelsen av galaxen. Astronomer är fram tills idag förbryllade över hur de hamnade där och hur de kommer att utvecklas över tid i sin bana kring galaxen. Något som forskare är säkra på är att den stjärntäta tunga disken hos Vintergatan drar i stjärnorna i de fjärran hoparna med sin gravitationskraft. Detta sker i den graden att de gamla stjärnorna från hoparna faktiskt lämnar stjärnhopen för att falla mot galaxen. Denna effekten existerar på grund av ett väldigt välbekant fenomen, som vi även ser här på jorden, nämligen tidvatteneffekten.

Så för att förstå hur stjärnhopar förlorar sina stjärnor under sin utveckling kan vi börja med att förstå hur tidvattenkrafter från vår måne påverkar våra hav i form av ebb och flod. Månen och jorden påverkar varandra konstant på grund av sina gravitationskrafter vilket resulterar i att de dras mot varandra. Eftersom jorden dras mot månen kommer allting som befinner sig på jorden att känna denna kraft (dock i olika grad med hänsyn till avståndet till månen) och om vi studerar större objekt (om jag får kalla hav "objekt" för sakens skull) kommer vi kunna se effekten av denna kraften som en rörelse mot månen. Vattnet som befinner sig rakt under månen kommer känna en starkare dragningskraft av månen jämfört med jordskorpan och vattnet på motsida klotet. Eftersom havet är i flytande form kommer det att kunna stretchas ut pekandes mot månen medans havet på motsatt sida av jorden kommer att känna en mindre dragkraft än jordskorpan och bli utdragen åt motsatt håll då den blir eftersläntande jämfört med resten av planeten. Detta skapar i sig en (inte så synlig) sfäroid form, som en amerikansk fotboll, runt jorden där havet på var sin sida är utdraget i vad vi uppfattar som flod.

Tidvatteneffekten som resulterar från att stjärnhoparna befinner sig i närheten av en väldigt massiv galax får stjärnorna att agera likt haven av månen. Likt vattnet stretchas hoparna till sfäroider pekandes mot galaxens centrum där de närmaste stjärnorna känner en starkare kraft än stjärnorna på motsatt sida hopen. Tidvattenkrafterna på strjärnhoparna är oftast så starka att stjärnor i spetsarna av sfäroidformen kan fly från hopen och dras istället mot galaxen. Denna förlust av stjärnor är en viktig del av stjärnhopars evolution och leder forskare till att studera ett fenomen ljusår borta genom att känna igen egenskaperna av det här på jorden.

I mitt arbete tittar jag på de evolutionära effekterna från dessa tidsvattenkrafter på stjärnhopar genom att applicera den relativt enkla idén av ebb och flod, som vi ser på jorden, i en ny metod. Denna nya metod kommer att kunna hjälpa oss förstå lite mer av vad som döljer sig bakom de mystiska himlakropparna vars förflutna fortfarande förbryllar forskare långt långt bortom Vintergatans glans.

Contents

1 Introduction **4**

2 Physical concepts and their implementations **7**
2.1 Version I: Balanced evolution in constant tidal fields 7
2.1.1 Equations describing the internal evolution 8
2.1.2 Prescription for the pre-core collapse evolution 12
2.1.3 Implementation 12
2.2 Version II: Unbalanced and balanced evolution in constant tidal fields . . . 15
2.2.1 Equations describing the evolution 15
2.2.2 Unbalanced phase 16
2.2.3 Balanced phase 18
2.2.4 Implementation 21
2.3 Version III: Arbitrary tidal fields 23
2.3.1 Potential escapers 23
2.3.2 Mode A 24
2.3.3 Mode B 24
2.3.4 Implementation 24
2.3.5 Proof of concept: elliptical orbits 26

3 Conclusions **29**

List of Figures

1.1 Picture of NGC 5907 with visible stellar streams, by 0.5-m Blackbird Remote Observatory telescope, 2006. 6

2.1 Version I simulations where the left column are figures for $\mathcal{R}_0 = 1/100$ and the right column are the results for $\mathcal{R}_0 = 1/30$. The values for the initial amount of stars in the cluster are included in the figures. Figures (a) and (b) shows the change in $\mathcal{R}$ (half-mass radius over Jacobi radius) over number of stars, figures (c) and (d) represent the normalized number of stars over time and figures (e) and (f) represent the normalized half-mass radius over time. 14

2.2 Version II simulations where the left column are figures for $\mathcal{R}_{hJ,0} = 1/100$ and the right column are the results for $\mathcal{R}_{hJ,0} = 1/5$. The values for the initial amount of stars in the cluster are included in the figures. Figures (a) and (b) represent the normalized number of stars over time, figures (c) and (d) represent half-mass radius over time and figures (e) and (f) represent form factor of the density profile over time. 22

2.3 Diagram describing the Jacobi surface, Lagrange points, bound stars and potential escapers. The energy E_J is the energy it takes to escape the cluster. Taken from Renaud [2018]. 23

2.4 Version III simulation for elliptical orbits. The figure shows the distance between galaxy and cluster over time. 26

2.5 Version III simulation for elliptical orbits. The plot shows the mass loss throughout the evolution. 27

List of Tables

2.1 Definition of variables for version I 10
2.2 Constants, description and set values for version I 11
2.3 Definition of variables for version II 19
2.4 Constants, description and set values for version II 20
2.5 Run time for simulations of different initial N 27

Chapter 1

Introduction

Star clusters as self gravitating, heavily star populated bodies, with ages sometimes older than galaxies, are great tools to understand the evolution of the Universe on cosmological time scales. Together with a good understanding of their formation and evolution and with observations of stellar streams, the star clusters can guide us through the formation of galaxies of different forms.

By following the evolution of star clusters, the configurations of stars distributed between cluster and galaxy can be traced as the stars move between their potentials. However, using current models for tidal forces from galaxies on clusters will neither make for accurate backward tracing nor be time efficient due to either

(i) large approximations (in fast numerical models) on cluster and galaxy interactions resulting in over-simplistic cases (e.g Alexander and Gieles [2012] which works in cases of isolated clusters or clusters with constant external influence)

(ii) or (in direct N-body models) computational challenges for hardware (e.g. when treating all forces acting on every star in the cluster), which leads to extremely slow simulations (e.g Wang et al. [2016] where results were expected after eleven months of simulating 10^6 bodies in a star cluster).

Due to these two factors, the challenge is to find a balance between constructing a very accurate numerical model while at the same time retain a computationally manageable scheme to produce valuable, fast simulations of star cluster evolution.

To accomplish an accurate model of star clusters both the internal and external dynamics of the cluster and galaxy system needs to be accounted for. The internal dynamics of the cluster is driven by interactions between stars, as well as their individual evolution. These bring the cluster through an *unbalanced phase* of mass segregation (section 2.2.2) and eventually *core collapse* (section 2.2.2), which leaves the cluster in a somewhat calmer future of *balanced evolution* (section 2.2.3). The keyword, for the internal dynamics, is *relaxation*, the process of finding the equilibrium of the system of stars as a whole as the energy is equiparted between all the stars.

The external dynamics refers to the interaction between galaxy and cluster. This is driven by the mass density profile of the galaxy as the cluster orbits the galactic centre.

Such things as spiral arms, disk formation, dark matter sub halos, galaxy merger situations and other structures make the potential quite complex and forbids the user to introduce approximations. The external dynamics leads the cluster stars to experience forces pulling them towards the local centre of gravity. The stars are thus experiencing the effects of the so called *tidal field* which is the net force resulting from the gravity of the galaxy and the cluster.

Accounting for both the external and internal dynamics can be done in direct N-body simulations, such as `NBODY6` (Aarseth [2003]) and `NBODY6tt` (Renaud et al. [2011]), meaning that influences on every star by the remaining $N - 1$ stars in the cluster are calculated separately at every iteration. However, as hinted at before, evaluating every force acting on every individual star is a massive computational challenge for any hardware and consumes up to months of computing time. Consequently, N-body simulations can be very accurate, however, the time-consuming process is not very appropriate for researchers trying to test out new galaxy models and gravitational potentials in a fast pace.

To circumvent the speed issue, faster methods have been proposed to solve the evolution of star cluster (Giersz et al. [2008] for a Monte-Carlo and Chernoff and Weinberg [1990] for a Fokker-Planck solution). The fastest are accomplished assuming the cluster as a single object being described by a few differential equations that can be solved using simple numerical integrators. Methods that have been used are for example Alexander and Gieles [2012] and Gieles et al. [2014] for a Runge-Kutta solution. However, all of these methods assume over-simplified constant tidal fields.

Assuming the cluster to act as a single object involves several approximations leading to a lack in good models describing tidal stripping in varying tidal fields. It is either not a good enough approximation for strong tidal fields (as in the case of Alexander and Gieles [2012]) and it is not compatible with varying potentials and is only useful in the cases of circular orbits about the galaxy. This is normally not the case considering clusters have cosmologically motivated non-circular orbits (meaning that the cluster will experience a varying potential due to other objects existing). If the numerical method would work for more complex orbits and tidal fields, then this method could be comparable in accuracy to the one of the N-body approach.

Star clusters in eccentric orbits lose their stars periodically as the tidal field grows stronger at shorter distances between cluster and galaxy center. The star loss is sometimes speculated to be symmetric about the pericentre of the orbit, which is not naturally the case. Star clusters accelerate some of their stars with an energy great enough to escape the cluster. However, these stars, called *potential escapers*, need to escape through one of the two Lagrange points positioned between the star cluster and the galaxy and behind the cluster in line with the galaxy (normally denoted L_1 and L_2 respectively). This results in the cluster containing a separate group of stars, that are not energetically bound to the cluster, but follow the same orbit about the galaxy. Due to the strong tidal field before the pericentre the probability of potential escapers fleeing through the Lagrange points is

greater. This means that most potential escapers will escape in this stronger tidal field. As the cluster crosses the point of the pericentre of its orbit it will not have had enough time to generate more potentially escaping stars and hence the loss of stars will not be symmetric about the pericentre (Renaud [2018]). This will give the loss of stars over time a more step-like behaviour which can be simulated with N-body simulations in e.g. Baumgardt and Makino [2003]. The concept of potential escapers would be of great significance if it was to be implemented into an already existing fast numerical method, meaning more complex tidal fields could be considered.

One relevant phenomena connected to star cluster evolution is stellar streams. These are the remnants of stars escaping star clusters over time and have been given their name because of how the stars belonging to them were lost relatively continuously over time in the orbit, creating a line of stars orbiting the galactic centre (figure 1.1).

One useful property of stellar streams is that they can help map the potential of the galaxy at different locations outside the galactic disk. This is otherwise difficult to predict due to the fact that an unknown amount of dark matter in the halo will make up the potential there. The stellar streams can be reproduced by star cluster evolution simulations as the lost stars, due to the presence of a tidal field, can be followed once they leave the cluster. Generating stellar streams with an accurate model of tidal forces could also help describe the gravitational potential to determine sub-structures of the dark halo.

Figure 1.1: Picture of NGC 5907 with visible stellar streams, by 0.5-m Blackbird Remote Observatory telescope, 2006.

In this project I have, with the help of an already existing numerical method together with the implementation of the concept of potential escapers, analyzed the evolution of mass loss of star clusters and studied whether this step-like behaviour, taking the physical shape of stars in groups in stellar streams (which are observed and studied in e.g. Just et al. [2009]), can be reproduced with a fast method. Having this method makes for a new approach which supplies researchers with fast computer simulations of star clusters in arbitrary tidal fields.

Chapter 2

Physical concepts and their implementations

The project uses an already existing fast numerical method to describe star cluster evolution. This will make up the basis on which the concept of potentially escaping stars are introduced to. By introducing the potential escapers we hoped to make the fast method more flexible to be able to use it to describe star clusters in any arbitrary tidal field. This means that the project is divided into three parts- the first two parts are produced by following Alexander and Gieles [2012] and Gieles et al. [2014] where the fast star cluster code Evolve Me A Cluster of StarS (`EMACSS`) is developed. After version II we will have a good approximation for star cluster evolution in constant tidal fields. Version III is developed upon the previous versions where the concepts of potential escapers and varying tidal fields are applied. `EMACSS` itself is not the code for which version III is built upon and was only run in the purpose of comparing version I and II of this project to results published in Alexander and Gieles [2012] and Gieles et al. [2014]. This fast numerical method was chosen because it resulted in a good learning experience for programming large scale simulations.

2.1 Version I: Balanced evolution in constant tidal fields

Version I was reproduced following Alexander and Gieles [2012] where the first version of `EMACSS` was presented. Star clusters generated by version I are evolving in constant tidal fields and the results only display the evolution after the core collapse of the cluster (see section 2.2.2). This is called the *balanced phase* of the cluster's evolution and is when the cluster has reached equilibrium after mass-segregation (where more massive stars move towards the center of gravity while the smaller stars migrate outwards) and will mostly only be affected by external forces.

Stellar evolution is not considered over the cluster evolution time. The stars are also approximated to be of the same mass making the mass of the entire cluster $M = Nm$,

where N is the number of stars in the cluster and m is the mass of one star. The galaxy in this model is approximated as a point mass object and the cluster is set on a circular orbit (i.e. constant tides).

The units are simplified for the sake of computational ease as $G = Nm = -4E = r_{\rm v} = 1$, where G is the gravitational constant, E is the total energy of the star cluster and $r_{\rm v}$ is the virial radius of the cluster (Heggie and Mathieu [1986]). The conversion to physical units is not needed for comparison to Alexander and Gieles [2012] and is not conducted during version I.

2.1.1 Equations describing the internal evolution

To come to terms with the differential equations used, it is important to understand where they come from. The important quantities of the star cluster that will be followed through every time step is the number of stars N, total energy of the cluster E and the half mass radius of the cluster r_h. The virial radius of the cluster, the radius at which the virial theorem is valid, is described by $r_v = -GM^2/(2W)$, where M is the total mass of the cluster, G is the gravitational constant and W is the potential energy of the cluster. By assuming that the cluster is in virial equilibrium throughout the evolution, the total energy is described by $E = W/2$. By solving for the potential energy in the expression for the virial radius and rewriting the expression for the total energy, we get the expression

$$E = \frac{W}{2} = -\frac{GM^2}{4r_v}. \tag{2.1}$$

In this version the virial radius is assumed to be the same as the half mass radius, $r_v = r_h$, by assuming the density profile remains constant throughout the evolution. Knowing that the total mass of the cluster is described by $M = Nm$ we get the following expression for the total energy

$$E = -\frac{GN^2m^2}{4r_h}. \tag{2.2}$$

Following the homologous model of Hénon [1969], we assume that the energy flux through a shell is equal to the change in energy inside the shell and go on to assume that the fraction of the total energy passing through the shell is constant per relaxation time. The relaxation time is the time that is required for the cluster to carry out the relaxation from a change in equilibrium back to equilibrium through star-star interactions. We have used the relaxation time within the radius enclosing half the mass of the cluster and it is defined as

$$\tau_{rh} = 0.138\frac{N^{1/2}r_h^{3/2}}{\sqrt{mG}\ln(\gamma N)} \tag{2.3}$$

as presented by Spitzer and Hart [1971], where $\gamma \approx 0.11$ (Giersz and Heggie [1994]) in the so called Coulomb logarithm. Following these assumption, an expression of the change

in total energy can be described by the half-mass relaxation time τ_{rh} and a dimensionless constant ζ describing the change in energy per half-mass relaxation time. This will take the form of

$$\frac{dE}{dt}\frac{1}{|E|} = \frac{\zeta}{\tau_{rh}}. \tag{2.4}$$

The differential equations describing the change in N and r are also described using their own dimensionless parameters and the half-mass relaxation time as

$$\frac{dN}{dt}\frac{1}{N} = -\frac{\xi}{\tau_{rh}} \tag{2.5}$$

$$\frac{dr_h}{dt}\frac{1}{r_h} = \frac{\mu}{\tau_{rh}} \tag{2.6}$$

where ξ is the dimensionless rate of escape and μ is the dimensionless rate of expansion. Considering the evolution of N is a negative, we expect ξ to be positive. To relate these three dimensionless variables together we can see that, from equation (2.2) where the energy change only depend on N and r_h, equation (2.4) can be written as

$$\begin{aligned}\frac{dE}{dt}\frac{1}{|E|} &= -\frac{Gm^2}{4}\left(\frac{2N}{r_h}\frac{dN}{dt} - \frac{N^2}{r_h^2}\frac{dr_h}{dt}\right)\left(\frac{4r_h}{Gm^2N^2}\right) \\ &= -\frac{dN}{dt}\frac{2}{N} + \frac{dr_h}{dt}\frac{1}{r_h}\end{aligned} \tag{2.7}$$

which can then be expressed as $\zeta = 2\xi + \mu$ and is the expression that couples the differential equations.

Jacobi surface and tidal radius

The Jacobi surface is the surrounding surface about the star cluster which determines the boundary at which stars experience a stronger acceleration by the host galaxy compared to the cluster. This means that stars belonging to the cluster that have sufficient kinetic energy to pass the Jacobi surface will leave the cluster and their bound state to orbit the galaxy independently from the cluster. The Jacobi surface goes through two points that are positioned in line with the cluster and galaxy, one between the cluster and the galaxy (L_1) and one outside the cluster-galaxy line (L_2), at the points where the effective potential, resulting from the mass of the cluster, the mass of the galaxy and its rotating framework, gives rise to a net acceleration of zero. These points are called Lagrange points and it is also through the Lagrange points from where the escaping stars will descend, either from L_1 and experiencing a stronger tidal field than the bound stars or through L_2 where they will experience a weaker tidal field than bound stars.

Realistically, the Jacobi surface results in a non spherical shape (Renaud et al. [2011]), however, in version I the Jacobi surface is approximated to be spherical with the Jacobi radius (also known as tidal radius)

$$r_J = R_G \left(\frac{GNm}{3M_G} \right)^{1/3}, \tag{2.8}$$

where R_G is the distance between the cluster and galaxy centre and M_G is the galaxy mass (King [1962]). This comes from the assumption that the cluster orbits in a circular motion about the galaxy, which is the case of clusters described by version I.

Constants, variables and coupling equations

The following tables describes the variables and constants used to determine ξ, ζ and μ. Details are provided in Alexander and Gieles [2012].

Table 2.1: Definition of variables for version I

Variable	Definition
E	Total energy
N	Total number of stars
m	Mean mass of all stars
r_h	Half-mass radius
ξ	Dimensionless rate of escape
μ	Dimensionless rate of expansion
τ_{rh}	Half-mass relaxation time
N_0	Initial number of stars
r_{h0}	Initial radius
r_J	Jacobi radius
$\mathcal{R}$	Ratio for radius to Jacobi radius
$\mathcal{R}_0$	Initial ratio for radius to Jacobi radius

Table 2.2: Constants, description and set values for version I

Constant	Definition	Value
γ	Constant in Coulomb logarithm	0.11
ζ	Fractional change in energy per half-mass relaxation time	0.111
G	Gravitational constant	1
ξ_1	Dimensionless escape rate for isolated cluster	0.0142
$\mathcal{R}_1$	Ratio of half-mass radius to Jacobi radius for Hénon (1965) models	0.145
N_1	Ideal cluster for which $\mathcal{R}_1$ is exactly correct	38 252
x	Variation of ξ with t_{rh}	0.75
z	Scaling of ξ with N around $\mathcal{R}_1$	1.61
f_N	Fractional change in N between start and time of core-collapse	0.95
f_r	Fractional change in r between start and time of core-collapse	1.81

The following equations describe the coupling equations that are presented by Alexander and Gieles [2012]. A function for a constant β was created to complement that only the ratio $\mathcal{R}$ between half-mass radius and Jacobi radius was given by Alexander and Gieles and not the actual galaxy mass and distance between galaxy and cluster, which will be of use in version III. β is therefore determined from combining equation (2.8) and that the ratio is $\mathcal{R}_0 = r_{h0}/r_{J0}$.

$$\mathcal{R} = \frac{\beta r_h}{(Nm)^{1/3}} \tag{2.9}$$

$$\beta = \frac{\mathcal{R}_0}{r_{h0}} (N_0 m)^{1/3} \tag{2.11}$$

$$\xi = \xi_1[1 - P(\mathcal{R}, N)] + \frac{3}{5}\zeta P(\mathcal{R}, N) \tag{2.10}$$

$$\mu = \zeta - 2\xi \tag{2.12}$$

$$P(\mathcal{R}, N) = \left(\frac{\mathcal{R}}{\mathcal{R}_1}\right)^z \left(\frac{N \ln(\gamma N_1)}{N_1 \ln(\gamma N)}\right)^{1-x} \tag{2.13}$$

Equation (2.13) is describing a probability $\mathcal{P}(\mathcal{R}, N)$ which will determine at which rate the mass loss will evolve as in equation (2.10). The probability will allow the escape rate to look different depending on whether the cluster has expanded to fill its Jacobi radius or not. In equation (2.13) $\mathcal{R}_1$, N_1, z and x are constants determined by Alexander and Gieles [2012] and are displayed in table 2.2.

2.1.2 Prescription for the pre-core collapse evolution

The pre-core collapse phase of a star cluster is driven by mass segregation, which is the exchange of kinetic energy between interacting stars which drives heavier stars to the center of the cluster while lighter stars are accelerated outward. This generally results in a rather short event compared to the entire life time of the cluster, leading Alexander and Gieles [2012] to focus mainly on the balanced evolution in their paper.

Alexander and Gieles treat the pre-core collapse phase through comparing their results with N-body simulations and evaluating the fraction of stars that have been lost and the fractional change in radius that has happened throughout the unbalanced phase. They evaluated the core-collapse to take place at about $20\tau_{rh,0}$ (20 times the initial half-mass relaxation time), at which point they would use a linear interpolation method to estimate the fractional changes. However, due to difficulties with reproducing this part of the method, an actual comparison to the `EMACSS` code itself was made where an empirical value of $13.513\tau_{rh,0}$ was instead found to be used. In this comparison it was also found that no fractional change was needed and the amount of stars lost in the unbalanced phase was not considered. Instead the initialized value of N would represent the number of stars after core collapse.

2.1.3 Implementation

The code was written in C++ language and implements all constants presented in table 2.2. It goes on to contain the differential equations (2.4), (2.5) and (2.6) as functions with τ_{rh}, their respective dimensionless variable ξ, μ or ζ and their current value of N, r_h or E as arguments. The differential equations are solved using a 4th order Runge-Kutta integrator that is implemented in the main file. It takes an adaptive time step ($0.1\tau_{rh}$ as presented by Alexander and Gieles), the current time, one of the differential equations' dimensionless variables, the previous value of N, r_h or E and one of the previously defined functions of the differential equations as arguments. The Runge-Kutta function then returns an updated value of either N, r_h or E.

The main function of the program reads an input file with the user defined values that will initialize the variables N, r_h and $\mathcal{R}$. To iterate through the star cluster evolution, a while-loop is used with the condition for the value of N not proceeding below 200 stars (the time of final dissolution and where the model is non valid due to the cluster being too small). A condition in case there would be a failure (e.g. strange initial values) is established, that follows that the while-loop must exit if a very large total time has passed. The first variables to be updated in the while-loop is the half-mass relaxation time and the coupling constants. The adaptive time step is then evaluated and the 4th order Runge-Kutta function is called three times, one time each for the three different differential equations.

The result presented in the output file was plotted together with the result of the N-body simulations produced by Alexander and Gieles [2012]. Six simulations were run to compare results to the N-body result presented in Alexander and Gieles [2012]. Three

simulations were run for $\mathcal{R}_0 = 1/30$ (i.e strong tides) where $N_0 = 1024$, 8192 and 65536 and three for $\mathcal{R}_0 = 1/100$ (i.e weak tides) with the same initial N. See comparison in figure 2.1. Results from running the `EMACSS` code can also be viewed in figure 2.1 due to the direct comparison that had to be conducted because of inconclusive results that did not match the N-body ones.

The initial plateau in sub figures (c) and (d) of figure 2.1 and (e) and (f) display $20\tau_{rh,0}$, representing the unbalanced evolution. This means that the mass loss during the unbalanced evolution was not accounted for in version I, rather that the initial number of stars and half mass radius presented by the user are the values at the time of the start of the balanced evolution. Looking at the plots, there is a noticeable difference in the evolution of the 1024 star cluster as conducted by `EMACSS` and the interpreted method. The difference is particularly visible in the case of the weaker tides. This could be due to misinterpretation of the prescription presented in Alexander and Gieles [2012]. We can already see a difference from the N-body results and the `EMACSS` results even though they should be roughly the same, showing the limitation in accuracy in the `EMACSS` code.

The typical expanding and contracting radius behaviour is first due to the relaxation driven expansion followed by shrinking because of energy lost du to tidal stripping (Hénon [1965])

Convinced that the main issue of the comparison comes from the interpretation of the compensated unbalanced phase, the decision to proceed to version II was made. It was at this point clear that a method including a model for the unbalanced phase and the core collapse was needed for a more realistic and conclusive model.

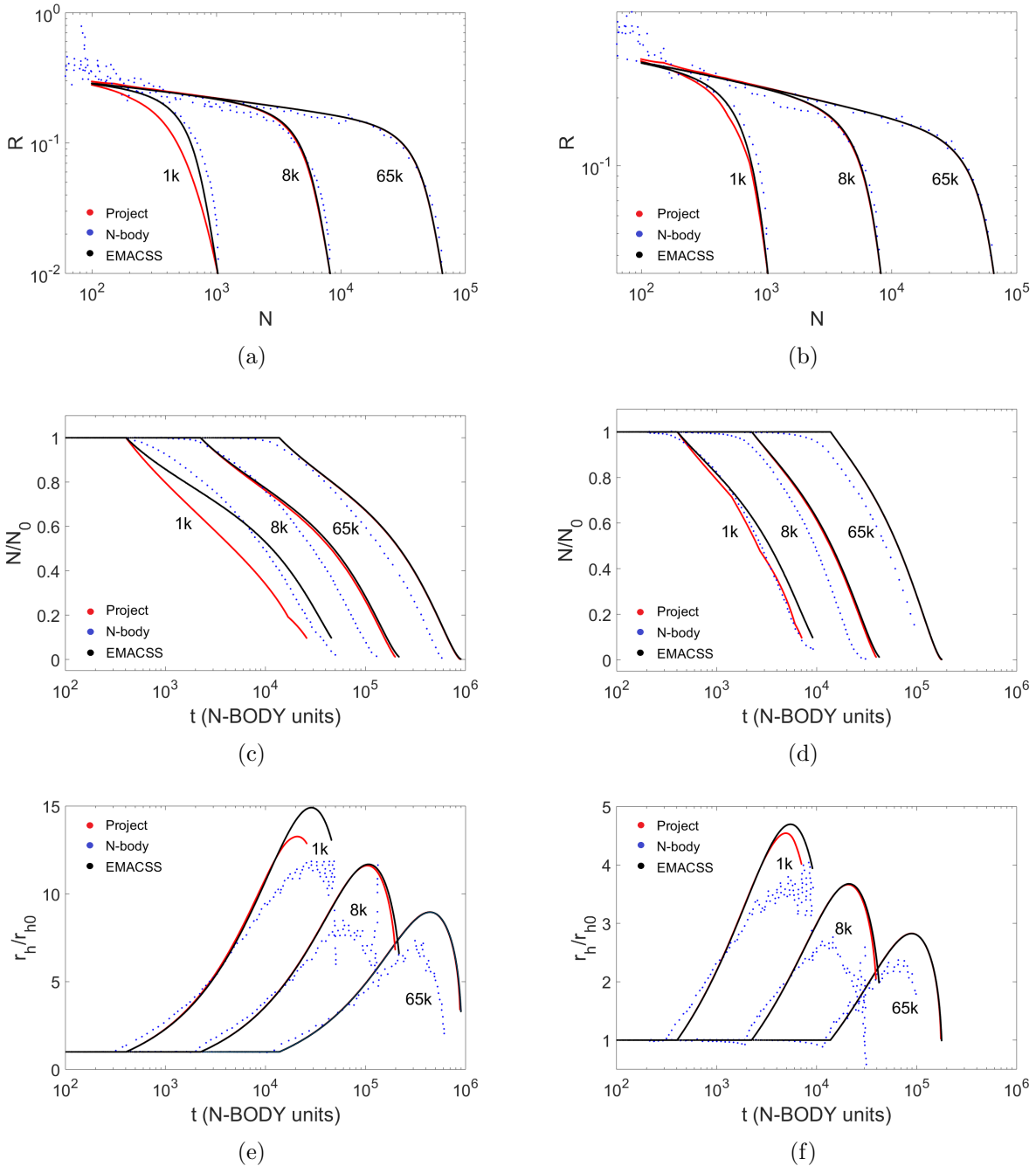

Figure 2.1: Version I simulations where the left column are figures for $\mathcal{R}_0 = 1/100$ and the right column are the results for $\mathcal{R}_0 = 1/30$. The values for the initial amount of stars in the cluster are included in the figures. Figures (a) and (b) shows the change in $\mathcal{R}$ (half-mass radius over Jacobi radius) over number of stars, figures (c) and (d) represent the normalized number of stars over time and figures (e) and (f) represent the normalized half-mass radius over time.

2.2 Version II: Unbalanced and balanced evolution in constant tidal fields

Version II, like version I, is an interpretation of an already published work. This version is based on Gieles et al. [2014], which presents the second version of their `EMACSS` code, that includes an investigation of the star cluster evolution prior to core-collapse as well as the post-core collapse evolution. As before, the star cluster evolution takes place in constant tidal fields, the stars are approximated to be of the same mass.

The main difference from version I when considering the earliest evolution of the star cluster is that the core parameters such as core radius r_c and core density ρ_c are significant parameters for the evolution, and are decoupled from the half-mass radius. The core parameters comes to play an important part as the core evolution will almost decouple from the entire cluster evolution. The central source of energy is explicitly the birth and the hardening of binaries in the core. This makes the form factor depending on the clusters density profile non constant (unlike version I) and will need to be considered for every iteration of the evolution. Recall from previous version that the form factor is what relates the virial radius to the half-mass radius determining somewhat the mass distribution of the cluster. Eventually, considering a vaying density profile leads us to consider two more differential equations describing the clusters evolution, one for the form factor κ and one for r_c.

2.2.1 Equations describing the evolution

The same differential equations as considered in version I are considered in version II as well. The only difference is that the change in total energy of the cluster does not remain constant throughout the entirety of the evolution as before when $\zeta = 0.111$. Here, we instead use the dimensionless parameter ϵ to describe the rate of change in total energy, where it takes the form $\epsilon \geq 0$ and $\epsilon \neq \zeta$ pre-core collapse and $\epsilon = \zeta$ during the post-core collapse, balanced, phase (Gieles et al. [2014]).

Because the unbalanced phase pre-core collapse causes the cluster to contract the form factor κ is no longer constant throughout the evolution. As mentioned before, the change in κ will now be described by a differential equation of the form as (2.5), (2.6) and (2.4). Its dimensionless rate of escape will be described by λ, which is expected to be $\lambda > 0$ for the pre-core collapse phase when the cluster is expected to contract and $\lambda < 0$ for the post-core collapse phase as the cluster dissolves (Gieles et al. [2014]).

The two updated differential equations can be written as

$$\frac{d\kappa}{dt}\frac{1}{\kappa} = \frac{\lambda}{\tau_{rh}} \tag{2.14}$$

$$-\frac{dE}{dt}\frac{1}{E} = \frac{\epsilon}{\tau_{rh}}. \tag{2.15}$$

In version II it is important that the half-mass radius and virial radius are distinct. This means that the expression for the total energy (2.1) instead takes the form

$$E = -\kappa\frac{GN^2m^2}{r_h}, \tag{2.16}$$

where we can see the new importance of the density profile form factor κ. Differentiating equation (2.16) gives

$$-\frac{dE}{dt}\frac{1}{E} = -\frac{d\kappa}{dt}\frac{1}{\kappa} + \frac{dr_h}{dt}\frac{1}{r_h} - \frac{dN}{dt}\frac{2}{N}, \tag{2.17}$$

where we instead get $\epsilon = -\lambda + \mu + 2$, which describes the new coupling of the differential equations.

2.2.2 Unbalanced phase

During the unbalanced phase, following the core evolution leading up to core collapse will be important since this will be decoupled from the entire cluster's evolution. This is due to mass segregation and kinetic energy being transferred outwards through interactions with lighter stars, leading to contraction of the massive central stars and forming a significant core of the cluster. The core radius r_c is therefore also introduced as a differential equation to follow throughout the evolution and particularly the pre-core collapse part. The equation takes the form

$$\frac{dr_c}{dt}\frac{1}{r_c} = \frac{\delta}{\tau_{rh}}$$

where δ is the dimensionless rate of core expansion. To relate δ to the other dimensionless variables Gieles et al. show that

$$\lambda = \mathcal{K}(\delta - \mu) \tag{2.18}$$

where

$$\mathcal{K} = \frac{\mathcal{R}_{ch}}{\kappa}\frac{2(\kappa_0 - \kappa_1)\exp(-\mathcal{R}_{ch}^2/\mathcal{R}_{ch0}^2)}{\sqrt{\pi}\mathcal{R}_{ch0}}. \tag{2.19}$$

Here κ_0 and κ_1 are reference values presented by Gieles et al. [2014], $\mathcal{R}_{ch} = r_c/r_h$ and $\mathcal{R}_{ch0} = r_{c0}/r_{h0}$ for the initial user defined values.

For the core evolution to be studied at a relevant time scale, a core relaxation time must be introduced (Spitzer and Hart [1971]):

$$\tau_{rc} = \frac{\sigma_c^3}{15.4G^2 m \rho_c \ln(\gamma N)} \tag{2.20}$$

where

$$\rho_c = \rho_{c0} r_c^{-\alpha}. \tag{2.21}$$

Here σ_c^2 is the mean-square velocity of stars in the core and follows $\sigma_c^2 = 8\pi G \rho_{c0} r_c^{2-\alpha}/3$. The power-law index was determined by Lynden-Bell and Eggleton [1980] to be $\alpha = 2.2$.

Of course the coupling equations for the unbalanced pre-core collapse phase take different forms compared to those presented in version I. They take the form

$$\delta = \delta_1 + \delta_2 \frac{\tau_{rh}}{\tau_{rc}} \tag{2.22}$$

$$\mu = \frac{(\mathcal{R}_{hJ}/\kappa)\xi_e + \mathcal{K}\delta}{1 + \mathcal{K}} \tag{2.23}$$

$$\mathcal{P} = \left(\frac{\mathcal{R}}{\mathcal{R}_1}\right)^z \left(\frac{N \ln(\gamma N_1)}{N_1 \ln(\gamma N)}\right)^{1-x} \tag{2.24}$$

$$\lambda = \mathcal{K}(\delta - \mu) \tag{2.25}$$

$$\xi = \mathcal{F}\xi_1(1 - \mathcal{P}) + (f + [1 - f]\mathcal{F})\frac{3}{5}\zeta\mathcal{P} \tag{2.26}$$

$$\mathcal{R} = \frac{\beta r_{\rm v}}{(Nm)^{1/3}} \tag{2.27}$$

$$\epsilon = -\lambda + \mu + 2\xi. \tag{2.28}$$

where δ_1, δ_2, ξ_1, f, N_1, x, z and $\mathcal{R}_1$ are constants displayed in table 2.4, $r_{\rm v}$ is the virial radius, β comes from equation (2.11) and $\mathcal{F} = \mathcal{R}_{ch}^{min}/\mathcal{R}_{ch}$ where $\mathcal{R}_{ch}^{min} = (N_2/N + N_2/N_3)^{2/3}$. This last part describing the fraction $\mathcal{F}$ defines the condition for core collapse to finally occur, as explained below.

Condition for core collapse

The transition between unbalanced to balanced evolution occurs as the star dense core region starts to create binary star systems that then accelerate stars interacting with them causing the cluster to expand. This constitutes the central source of energy that stops the collapse and allows to reach the balanced phase described by Hénon [1965]. Since the interactions between stars are not explicitly studied in this method, Gieles et al. [2014] suggest the transition to occur when

$$\mathcal{R}_{ch}^{min} = \left(\frac{N_2}{N} + \frac{N_2}{N_3}\right)^{2/3} \geq \frac{r_c}{r_h}, \tag{2.29}$$

where N_2 and N_3 are constant determined by Gieles et al. [2014] and are given in table 2.4. The condition means that $\mathcal{F}$ from equation (2.26) makes the transition between the

unbalanced form $f(3/5)\zeta\mathcal{P}$ into the balanced form that is equation (2.10) smooth as it proceeds to become almost unity as core collapse approaches. When core collapse has been reached, $\mathcal{R}_{ch}^{min}$ is no longer needed for the balanced phase and the comparison is abandoned, leaving $\mathcal{F} \approx 1$ for the rest of the evolution.

2.2.3 Balanced phase

The post-core collapsed phase is called the balanced phase in version II and introduces some slight changes to the coupling equations compared to version I. To start, equation (2.10) is used to describe ξ however this time with equation (2.24) describing $\mathcal{P}$. The other coupling equations take the form of

$$\mu = \zeta + \left(\frac{2}{3}\mathcal{K}\left[1 + \frac{N}{N_3}\right]^{-1} - 2\right)\xi \quad (2.30) \qquad \lambda = \mathcal{K}(\delta - \mu) + \frac{\kappa(\mathcal{R}_{ch}) - \kappa}{\kappa(\mathcal{R}_{ch})} \quad (2.32)$$

$$\delta = \frac{2}{3}\xi\left(1 + \frac{N}{N_3}\right)^{-1} + \mu \quad (2.31) \qquad \kappa(\mathcal{R}_{ch}) = \kappa_1 + (\kappa_0 - \kappa_1)\mathrm{erf}\left(\frac{\mathcal{R}_{ch}}{\mathcal{R}_{ch0}}\right) \quad (2.33)$$

The evolution of ϵ is now constant and set to $\epsilon = \zeta$ like in version I.

To follow the evolution of the core in the balanced phase, the density is now defined as

$$\rho_c = \left(\frac{r_c}{r_h}\right)^{-2}\frac{3Nm}{8\pi r_h^3}. \quad (2.34)$$

Constants and variables

The differential equations used in version II can be written as and will be used in the form

$$\frac{dN}{dt} = -\frac{\xi}{\tau_{rh}}N \quad (2.35) \qquad \frac{dE}{dt} = -\frac{\epsilon}{\tau_{rh}}E \quad (2.37)$$

$$\frac{dr_h}{dt} = \frac{\mu}{\tau_{rh}}r_h \quad (2.36) \qquad \frac{d\kappa}{dt} = \frac{\lambda}{\tau_{rh}}\kappa \quad (2.38)$$

$$\frac{dr_c}{dt} = \frac{\delta}{\tau_{rh}}r_c. \quad (2.39)$$

The following tables describes the variables and constants used to determine the coupling variables.

Table 2.3: Definition of variables for version II

Variable	**Definition**
E	Total energy
N	Total number of stars
m	Mean mass of stars
κ	Form factor depending on density profile
$r_{\rm v}$	Virial radius
r_c	Core radius
r_h	Half-mass radius
ξ	Dimensionless rate of escape
μ	Dimensionless rate of expansion
ϵ	Dimensionless rate of change of energy
λ	Dimensionless variable for form factor
δ	Dimensionless variable for core evolution
N_0	Initial number of stars
r_{h0}	Initial half-mass radius
$\mathcal{R}_{ch}$	Ratio for core radius to half-mass radius
$\mathcal{R}_{hJ}$	Ratio for half-mass radius to Jacobi radius
$\mathcal{R}$	Ratio for virial radius to Jacobi radius
R_{hJ0}	Initial ratio for half-mass radius to Jacobi radius
τ_{rh}	Half-mass relaxation time
τ_{rc}	Core relaxation time
σ_c^2	Mean-square velocity of stars in core
ρ_c	Core density
ρ_r	Mean density within r_h
ρ_0	Central density

Table 2.4: Constants, description and set values for version II

Constant	**Definition**	**Unbalanced**	**Balanced**
ζ	Fractional change in energy per half-mass relaxation time	0.1	0.1
δ_1	Dimensionless rate of initial core contraction speed	-0.09	
δ_2	Dimensionless rate of core collapse	-0.002	
ρ_{c0}	Proportionality constant for core density	0.055	
α	From Lyden-Bell et al. (1980) and Heggie et al. (1988)	2.2	
$\mathcal{R}_{ch0}$	Initial rate for core radius to half-mass radius	0.100	0.220
κ_0	Initial form factor depending on density profile	$r_h/(4r_v)$	0.200
κ_1	Reference value of form factor	0.295	0.265
f	Escape rate of Roche volume filling clusters	0.3	
ξ_1	Escape rate for isolated clusters	0.0142	0.0142
x	Variation of ξ_e with τ_{rh}	0.75	0.75
z	Scaling of ξ_e with N around $\mathcal{R}_{\mathrm{v}J1}$	1.61	1.61
$\mathcal{R}_1$	Ratio of virial radius to Jacobi radius for Hénon (1961) models	0.145	0.145
N_1	Ideal cluster for which $\mathcal{R}_{\mathrm{v}J1}$ is exactly correct	15000	15000
N_2	Constant important for core evolution		12
N_3	Boundary for clusters evolving either as $N^{-2/3}$ or constant		15000

2.2.4 Implementation

The code for version II is constructed in a similar way to version I. The common equations for the unbalanced and balanced phase, which are (2.3), (2.9), (2.20), (2.27) and $r_{\rm v} = r_h/(4\kappa)$, are defined and declared. There are two different versions for calculating $\mathcal{R}_{ch}$, one denoted with N and one with r, as follows

$$\mathcal{R}_{ch}^{N} = \left(\frac{N_2}{N} + \frac{N_2}{N_3}\right)^{2/3} \tag{2.40}$$

$$\mathcal{R}_{ch}^{r} = \frac{r_c}{r_h}. \tag{2.41}$$

Comparing (2.40) and (2.41) allows to define the transition between the two phases.

For this version, the user provides the initial value of N, r_h, r_c, $\mathcal{R}_{hJ}$ and κ. The time steps in this phase are now a combination of τ_{rh} and τ_{rc} (Gieles et al. [2014]) as

$$\Delta t = [(100\tau_{rc})^{-1} + (0.1\tau_{rh})^{-1}]^{-1}. \tag{2.42}$$

This is to be able to update the variables correctly on a core relaxation time scale. The variables N, r_h, E, κ and r_c are updated using their differential equations and the Runge-Kutta integrator.

The result presented in the output file is plotted together with the result of the N-body simulations produced by Gieles et al. [2014]. Six simulations were run to compare to the N-body results. Three simulations were run for $\mathcal{R}_0 = 1/5$ where $N_0 = 4096$, 16384 and 65536, $\kappa_0 = 0.205$ and $r_{h0} = 0.82$ and three for $\mathcal{R}_0 = 1/100$ with the same initial N, $\kappa_0 = 0.195$ and $r_{h0} = 0.78$. See comparison in figure 2.2. The reason for the different values of κ is due to what model suits the situation best. In the case of a weak tidal field, a Plummer model with an infinit potential is the most appropriate (Plummer [1911]) because the potential of the cluster is still influential on the system. In the case of a strong tidal field, a King model, with a truncated star distribution (King [1966]), is better because the external potential will be much more dominant over the cluster's outside the tidal limit of the cluster.

The comparison to the N-body simulations conducted by Alexander and Gieles [2012] is simpler in this version. This is most likely due to the interpretation of the prescription is more correct compared to version I.

We can see in figure 2.2 for the stronger tidal field ((b), (d) and (f)) how there now is a distinct boundary for where the core collapse takes place. For the weaker tidal field it is not as visible however it makes sense that the stronger tidal field would much quicker strip the stars off the cluster. We still see the characteristic expansion and contraction of the cluster in the balanced phase and as expected, in both tidal cases, the form factor κ goes up during the unbalanced phase and decreases with the dissolution.

This method is very good to describe star cluster evolution in constant tidal fields, however, to move towards a method that can also consider elliptical orbits, the concept of potentially escaping stars needs to be added.

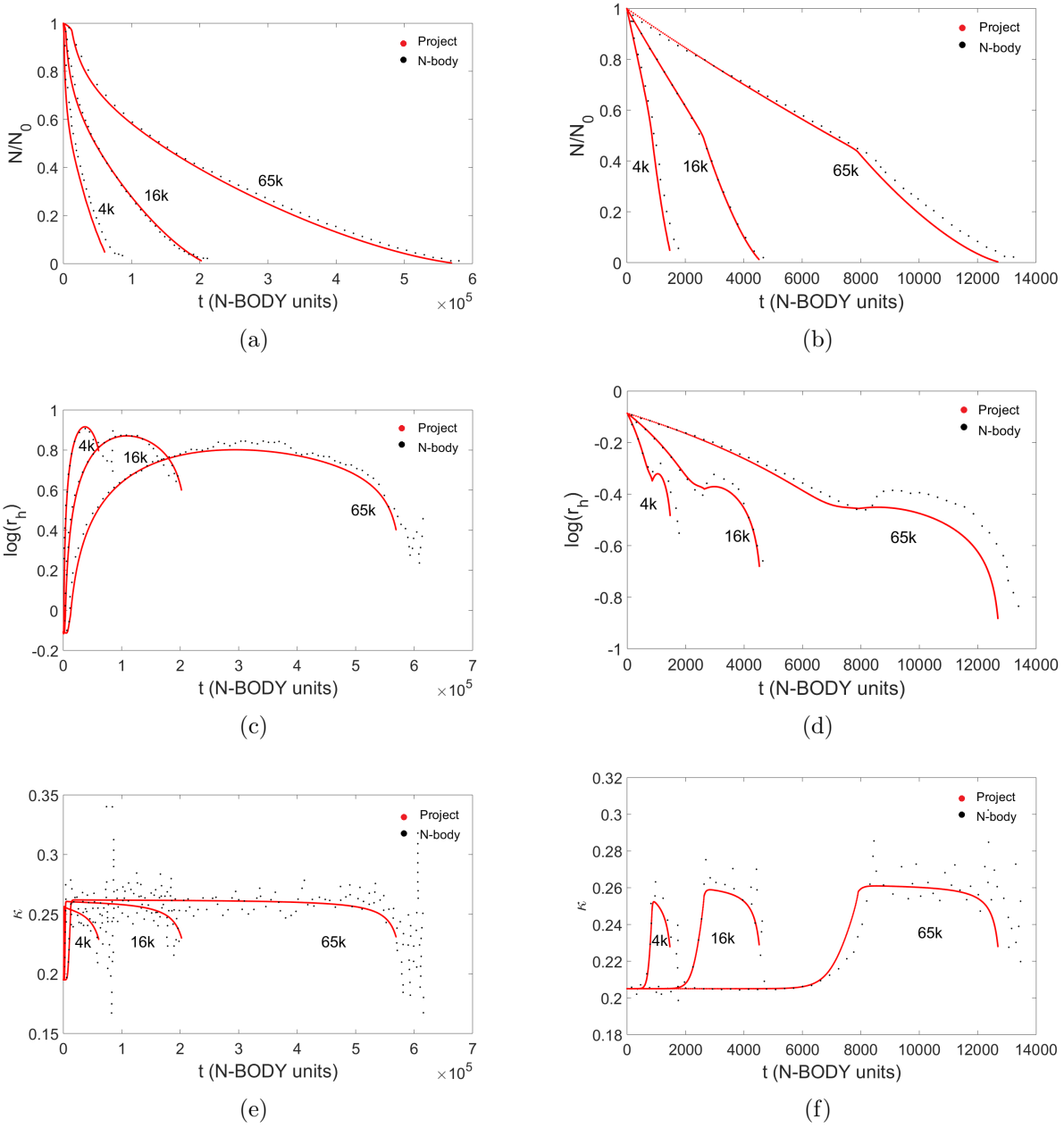

Figure 2.2: Version II simulations where the left column are figures for $\mathcal{R}_{hJ,0} = 1/100$ and the right column are the results for $\mathcal{R}_{hJ,0} = 1/5$. The values for the initial amount of stars in the cluster are included in the figures. Figures (a) and (b) represent the normalized number of stars over time, figures (c) and (d) represent half-mass radius over time and figures (e) and (f) represent form factor of the density profile over time.

2.3 Version III: Arbitrary tidal fields

Version III is based upon the interpretation and procedure which is version II and is the result of a combination of methods presented in Renaud et al. [2011] and Renaud and Gieles [2015] to treat tides. This version will give the user the possibility of entering any external potential (defined by a function of space or constructed from an independent cosmological simulation) to act on the star cluster. The method is developed so that the user feeds the program the initial values of N, r_h, κ and the external potential in physical units, however, the units are converted to N-body units for simplicity.

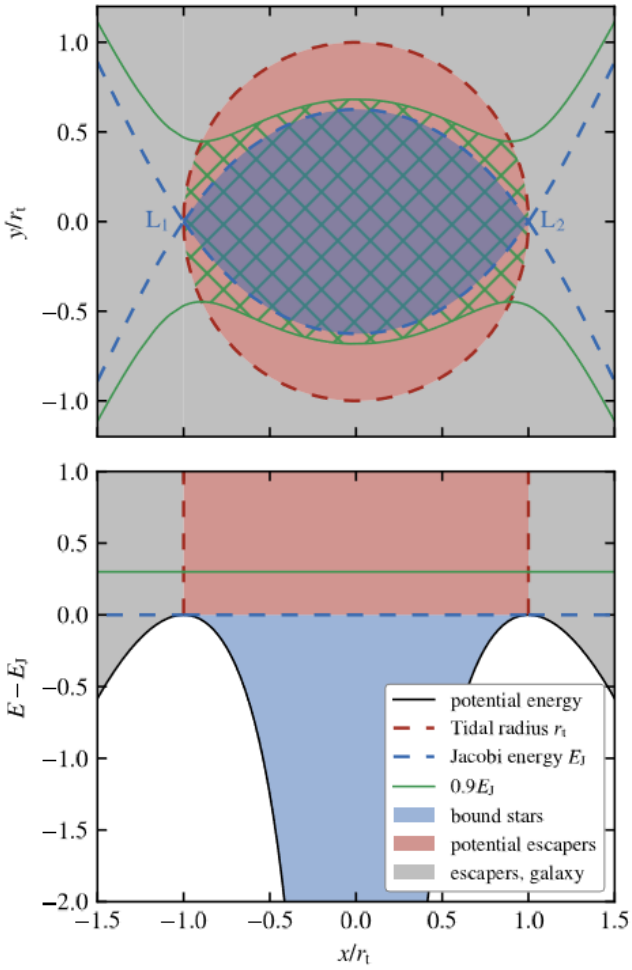

Figure 2.3: Diagram describing the Jacobi surface, Lagrange points, bound stars and potential escapers. The energy E_J is the energy it takes to escape the cluster. Taken from Renaud [2018].

2.3.1 Potential escapers

Potential escapers, as mentioned in the introduction, are stars that have gained enough energy to escape the cluster but have yet to exit beyond the tidal radius through the Lagrange points (first described by Hénon [1969]). These belong to an individual population of stars separate from the bound stars, which means that potential escapers have never been explicitly distinguished from other stars in previous methods. They are often disregarded and thought of as escaped stars (and accounted for by a fitted parameter in version I and II, in the only case of constant tides). To regard their properties and contribution to the mass loss of star clusters, potential escapers need to be integrated individually (through e.g. a N-body approach). Version III does just this - the approach presented by Gieles et al. [2014] is used to describe the bound stars, (i.e. the stars with negative energy), assuming that the tidal field is constant over the time step. This allows relaxation and simplified tides to accelerate some stars to posi-

tive energies. These become potential escapers and are described by a separate integrator method where the tidal field is treated more precisely. This dual treatment allows for the fast evolution of the bound part of the cluster (as in version I and II), and a much more accurate treatment of tidal stripping with potential escapers, without the prohibitive cost of the full N-body model.

In figure 2.3 (only studying the above most figure), the red area represents the area in which the potential escapers exist. This is within the tidal radius ($r_{\rm J}$), even though it surpasses the limit of the escape energy (blue dotted line called Jacobi energy in the figure). An example of $0.9E_{\rm J}$ is shown in orange, describing what could be a potential escaper's region of occupancy (recall that $r_{\rm J}$ is negative).

2.3.2 Mode A

Mode A is one of the two methods to help determine the acceleration at any point in the evolution of the cluster and is based on Renaud et al. [2011]. It needs to be fed a file (resulting from a previously made cosmological simulation) that contains the tidal tensor along an orbit. This information fully describes the tidal field at these positions. The code then uses a polynomial interpolation to recover the acceleration in the point in which the cluster is arbitrarily positioned.

The star cluster is positioned at origin and the method positions it in the external potential which will evolve around the origin.

Mode A allows for arbitrary complex tides, e.g those of a galaxy merger (Renaud and Gieles [2013]). However, it only tracks the tides on a pre-computed orbit, and thus does not allow for following stars far from the position of the cluster (e.g. in streams). A second mode has been developed to fix this issue.

2.3.3 Mode B

Mode B defines the galactic potential as a function of time and space. It is based on Renaud and Gieles [2015] and uses a differential method to integrate the star cluster motion about the galaxy. For this mode, there is no need for a prior cosmological simulation to get the potential and the tidal acceleration can be computed at any time during the simulation whenever it is needed. This model is thus limited to what can be described by a function of the external potential.

2.3.4 Implementation

Version III is built on version II with the addition of introducing potential escapers evolving along with the cluster in the main while-loop. The information about the potential escapers is stored dynamically in the form of a linked list. A linked list is created using an object of the class `Node`. The node-class has two important private members declared - one where relevant data will be stored and one pointer to another node object. This means that when a new node object is declared, it needs to be given the relevant data and the address of

the previous node so that it is not lost in the memory. The first node to be introduced will have the link to a null pointer, noting the beginning of the linked list. In our case, the data part of the object is an array of length 11, meaning it will fit three coordinates, the velocity and acceleration vectors, one boolean variable determining the state (potentially escaping or escaped) of the potential escaper and an index number.

The potential escapers are produced by the energy lost by the cluster and once a potential escaper is stored, a function generating a random position at a distance of r_h from the cluster center and a random velocity is called. The random velocity comes from the expression $E_k = 1/2V + E_p$ where E_k is the kinetic energy and E_p is the potential energy of the star. From this point, the potential escaper will evolve in the current potential using a leap-frog integrator method. The choice of a leap-frog integrator is mainly for computational speed sake, where accuracy is not the main focus, there will be a lot of potential escapers generated and iterated over, it is not possible to use a more advanced integrator method.

A function that determines whether the potential escaper has escaped the cluster or not takes in a user defined parameter that gives a multiple of r_J, which will determine at what distance the escaping star will finally be able to flee the cluster from. This is similar to what is commonly done in N-body simulations.

Depending on the user's input parameters, the program determines if mode A or mode B is to be used. In the main while loop, the tidal acceleration is computed at the current cluster position. The energy before being updated through the call to the 4th order Runge-Kutta function is compared to the updated one, deciding the energy loss at the time step. The number of stars being lost at the time step is also stored in order to determine the amount of potential escapers coming to existence. The leap-frog function is called for every iteration to update the position of every potential escaper.

For this version, the user is expected to input initial value of N, r_h, r_c and κ and depending on the user, either the initial coordinates and velocity vector for the cluster or complement with a previously determined tensor description of the external potential. The time step was chosen to be 0.001 times the adaptive time step used in version II. The program returns an outputfile with the updated values resulting from the Runge-Kutta integration and the total time.

2.3.5 Proof of concept: elliptical orbits

In figure 2.4 and 2.5 the results are displayed after one simulation of initial condition $N = 4096$, $r_h = 0.78$, $r_c = 0.32$, $\kappa = 0.195$ (using a model of Plummer [1911] to describe the cluster distribution) and $cr_{\text{J}} = 500r_{\text{J}}$ (where c is some constant determined at initialization). Mode B was used and hence the initial position of the cluster was initiated at $[1, 0, 0]$ kpc (for position vector $[x, y, z]$) and $[0, 100, 0]$ km/s (for velocity vector $[v_x, v_y, v_z]$). These initial coordinates and velocity vectors were chosen mainly to exaggerate the tidal influence on the cluster and is not a necessarily a realistic orbit of a star cluster about the galactic centre. The orbit was chosen mainly for the purpose of showcasing the step-like behaviour of mass loss.

The galactic mass was set to be 10^{10} solar masses. Like version I and II the potential of the galaxy was chosen to be the one of a point mass.

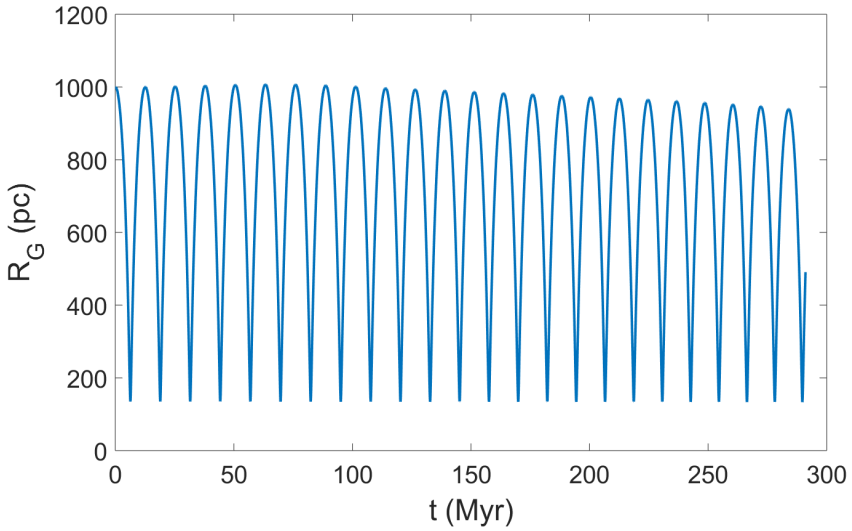

Figure 2.4: Version III simulation for elliptical orbits. The figure shows the distance between galaxy and cluster over time.

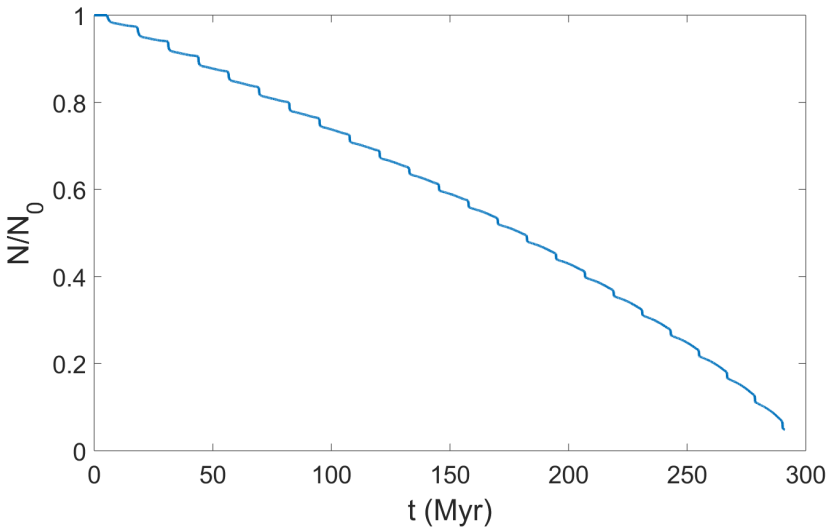

Figure 2.5: Version III simulation for elliptical orbits. The plot shows the mass loss throughout the evolution.

The initial conditions results in a elliptical orbit with eccentricity of about 0.7. In figure 2.4 the distance from the cluster to the galaxy (here denoted R_G) can be observed. In figure 2.5, the mass loss over time is displayed. Observing plot 2.4 and 2.5, we can observe that every sudden loss of stars (as in the stair case like behaviour) happens about the shortest R_G. This means that the most stars are lost at about the pericentre as expected. This is a great result, showing that even though our model is simplified, the staircase behaviour in mass loss can be reproduced.

In figure 2.4 we can see a slight decrease in the distance from the cluster to the galactic centre. This is not expected and was most probably due to a too large time step being used for updating the potential of the galaxy. This might lead to a change in orbit and if the project was to be extended, this could be looked into more carefully.

Table 2.5: Run time for simulations of different initial N

N	Run time (approximate)
1000	9 sec
4000	37 sec
8000	1 min 30 sec
16000	4 min 20 sec

This simulation took about 37 seconds to preform. Times taken for three other different simulations with different initial N are displayed in table 2.5. The result of 90 seconds for a 8000 star simulation on an Intel Core i5 processor can be compared to one simulation conducted in Renaud et al. [2011] with `NBODY6TT`, which reportedly took about six hours to preform using a GPU acceleration.

The value of $500r_\mathrm{J}$ was chosen for the simulation to possibly see a greater effect of the stair-like behaviour. This value was arbitrarily chosen, however a large value might help compensate for the fact that potential escapers need to flee through only the Lagrange points and not only at the distance of cr_J, which is the case at the moment. If more time was available, there could be a chance of developing a good strategy for compensating for this escape probability. However, at this point, the cr_J method shows the effects of varying tidal fields.

An extension of the project would be to have a more detailed comparison to version II, as well as a comparison to the results presented in e.g. Renaud et al. [2011] where a direct N-body method was used.

Chapter 3

Conclusions

Adding the concept of potential escapers improves the accuracy of the existing numerical methods and allows to head towards a more realistic model of mass loss in star clusters. The results now show the step-like mass loss behaviour which is expected due to the cluster experiencing different strength of the tidal field throughout its orbit about the galactic centre. Hence, these results can be compared to N-body simulations which can also take elliptical orbits or other in-homogeneous potentials into consideration. However, compared to the N-body simulation, this method allows the user to receive results after several seconds or up to a few minutes, depending on the simulation, which will allow the user to try out multiple conditions for a simulation in one hour of research time. Seeing this promising result, I believe that more time should be invested in optimizing this method (e.g change the adaptive time step for the potential escaper integration).

The most significant reason this fast numerical approach is more accurate than other fast methods (e.g. Giersz et al. [2008], Vasiliev [2016] and Gieles et al. [2014]) is due to the fact that it can position any massive star cluster (e.g. between 1000 and 65000 stars as used in this project) in any potential about a galaxy, leaving the cluster in any shape of an orbit. This flexibility has not yet been possible since most numerical methods only allow circular orbits, however, we know that complex orbits are more realistic and it is important to evolve star clusters in non-circular orbits.

The accuracy of the method can be significantly improved by considering the evolution of stars within the simulated cluster. This would include different mass stars unlike the method used in version III where we only considered single mass stars. This is important in the theory behind the internal forces driving the evolution of the cluster. Stars are interacting through relaxation and considering the probability of binary stars existing and interacting with other cluster stars is important if we want to study an accurate picture of the evolution. For this to be considered, we need updated versions of the coupling equations and a differential equation describing the mean mass of the stars in the cluster. This will be relevant since the mean mass will be changing with the loss of different mass stars. Theories like this exist (e.g. Alexander et al. [2014]) and it would take little time to implement into the current version presented in this project.

Another improvement that could be done to increase the accuracy of these results would be to consider a more relevant time step for version III. At the moment, the cluster is evolving at an arbitrary small time step (about 0.001 of the adaptive step size used in version II), not adapted to each iteration. This could have been worked on if more time was available for the duration of this project. A series of tests with different fractions of the previously used time step could have been tried out to reach highest time efficiency. However, for proving the concept's validity, the current time step is sufficient since it is showing a result much like the N-body simulation's (e.g Renaud et al. [2011] and Renaud and Gieles [2015]).

The implementation of the potential escapers is still very simple even though it is showing high efficiency. The leap-frog method is of the second order for computational speed sake, however, if more computational power was to be provided to the simulation, a more accurate integrator could be used. In the same leap-frog integrator function, the time step is the same of the star cluster Runge-Kutta integrator, which means that the time step used to evolve the motion of the potential escapers is not consistent throughout the entire evolution. This is not optimal and fixing this would be another step in the further improvement of this model.

The method of describing star clusters as single systems implemented with the concept of potential escapers in any tidal field can be relevant to many case studies. Considering any large body made up of tightly bound stars, like massive star clusters and some dwarf galaxies, will be possible with this model. This will give researchers much freedom to explore new concepts, try out models considering different formations of matter and dark matter in the external potential and not have to worry about computational restrictions on the hardware. The possibilities can only be imagined of having the power to run millions of different simulations of this sort on any super computer over the course of 24 hours.

Bibliography

Florent Renaud. Star clusters in evolving galaxies. *New Astronomy Reviews*, 81:1–38, April 2018. doi: 10.1016/j.newar.2018.03.001.

Poul E. R. Alexander and Mark Gieles. A prescription and fast code for the long-term evolution of star clusters. *MNRAS*, 422:3415–3432, June 2012. doi: 10.1111/j.1365-2966.2012.20867.x.

Long Wang, Rainer Spurzem, Sverre Aarseth, Mirek Giersz, Abbas Askar, Peter Berczik, Thorsten Naab, Riko Schadow, and M. B. N. Kouwenhoven. The DRAGON simulations: globular cluster evolution with a million stars. *MNRAS*, 458:1450–1465, May 2016. doi: 10.1093/mnras/stw274.

Sverre J. Aarseth. *Gravitational N-Body Simulations*. 2003.

Florent Renaud, Mark Gieles, and Christian M. Boily. Evolution of star clusters in arbitrary tidal fields. *MNRAS*, 418:759–769, December 2011. doi: 10.1111/j.1365-2966.2011.19531.x.

Mirek Giersz, Douglas C. Heggie, and Jarrod R. Hurley. Monte Carlo simulations of star clusters - IV. Calibration of the Monte Carlo code and comparison with observations for the open cluster M67. *MNRAS*, 388:429–443, July 2008. doi: 10.1111/j.1365-2966.2008.13407.x.

David F. Chernoff and Martin D. Weinberg. Evolution of Globular Clusters in the Galaxy. *ApJ*, 351:121, March 1990. doi: 10.1086/168451.

Mark Gieles, Poul E. R. Alexander, Henny J. G. L. M. Lamers, and Holger Baumgardt. A prescription and fast code for the long-term evolution of star clusters - II. Unbalanced and core evolution. *MNRAS*, 437:916–929, January 2014. doi: 10.1093/mnras/stt1980.

Holger Baumgardt and Junichiro Makino. Dynamical evolution of star clusters in tidal fields. *MNRAS*, 340:227–246, March 2003. doi: 10.1046/j.1365-8711.2003.06286.x.

A. Just, P. Berczik, M. I. Petrov, and A. Ernst. Quantitative analysis of clumps in the tidal tails of star clusters. *MNRAS*, 392:969–981, January 2009. doi: 10.1111/j.1365-2966.2008.14099.x.

D. C. Heggie and R. D. Mathieu. *Standardised Units and Time Scales*, page 233. 1986. doi: 10.1007/BFb0116419.

M. Hénon. Rates of Escape from Isolated Clusters with an Arbitrary Mass Distribution. *A&A*, 2:151, June 1969.

Jr. Spitzer, Lyman and Michael H. Hart. Random Gravitational Encounters and the Evolution of Spherical Systems. I. Method. *ApJ*, 164:399, March 1971. doi: 10.1086/150855.

M. Giersz and D. C. Heggie. Statistics of N-Body Simulations - Part One - Equal Masses Before Core Collapse. *MNRAS*, 268:257, May 1994. doi: 10.1093/mnras/268.1.257.

Ivan King. The structure of star clusters. I. an empirical density law. *AJ*, 67:471, October 1962. doi: 10.1086/108756.

M. Hénon. Sur l'évolution dynamique des amas globulaires. II. Amas isol&eacute. *Annales d'Astrophysique*, 28:62, February 1965.

D. Lynden-Bell and P. P. Eggleton. On the consequences of the gravothermal catastrophe. *MNRAS*, 191:483–498, May 1980. doi: 10.1093/mnras/191.3.483.

H. C. Plummer. On the problem of distribution in globular star clusters. *MNRAS*, 71:460–470, March 1911. doi: 10.1093/mnras/71.5.460.

Ivan R. King. The structure of star clusters. III. Some simple dynamical models. *AJ*, 71:64, February 1966. doi: 10.1086/109857.

Florent Renaud and Mark Gieles. A flexible method to evolve collisional systems and their tidal debris in external potentials. *MNRAS*, 448:3416–3422, April 2015. doi: 10.1093/mnras/stv245.

F. Renaud and M. Gieles. The role of galaxy mergers on the evolution of star clusters. *MNRAS*, 431:L83–L87, April 2013. doi: 10.1093/mnrasl/slt013.

Eugene Vasiliev. Evolution of binary supermassive black holes and the final-parsec problem. In Y. Meiron, S. Li, F. K. Liu, and R. Spurzem, editors, *Star Clusters and Black Holes in Galaxies across Cosmic Time*, volume 312 of *IAU Symposium*, pages 92–100, February 2016. doi: 10.1017/S1743921315007607.

Poul E. R. Alexander, Mark Gieles, Henny J. G. L. M. Lamers, and Holger Baumgardt. A prescription and fast code for the long-term evolution of star clusters - III. Unequal masses and stellar evolution. *MNRAS*, 442:1265–1285, August 2014. doi: 10.1093/mnras/stu899.